Microstructural Evolution Study of Battery Electrode Materials using TXM

Jun Wang

Physicist, Spokesperson X8C TXM Beamline

Workshop of Complex Functional Materials: Probing the Meso-Scale Structural Organization and the System Dynamics with Soft X-ray

U.S. DEPARTMENT OF ENERGY

BROOKHAVEN NATIONAL LABORATORY

BROOKHAVEN SCIENCE ASSOCIATES

Transmission X-ray Microscopy

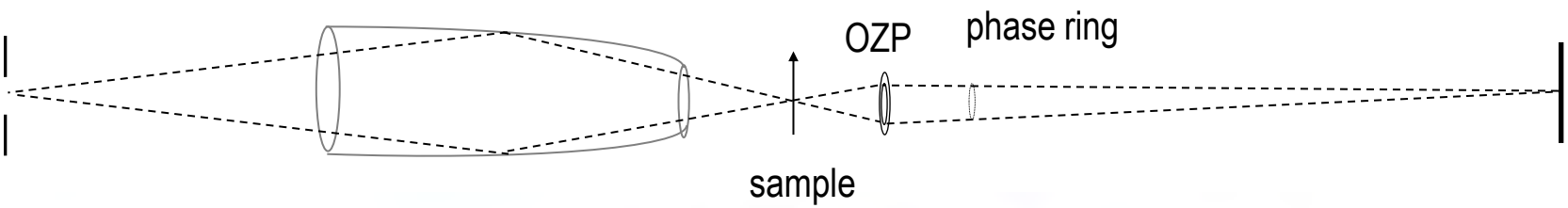

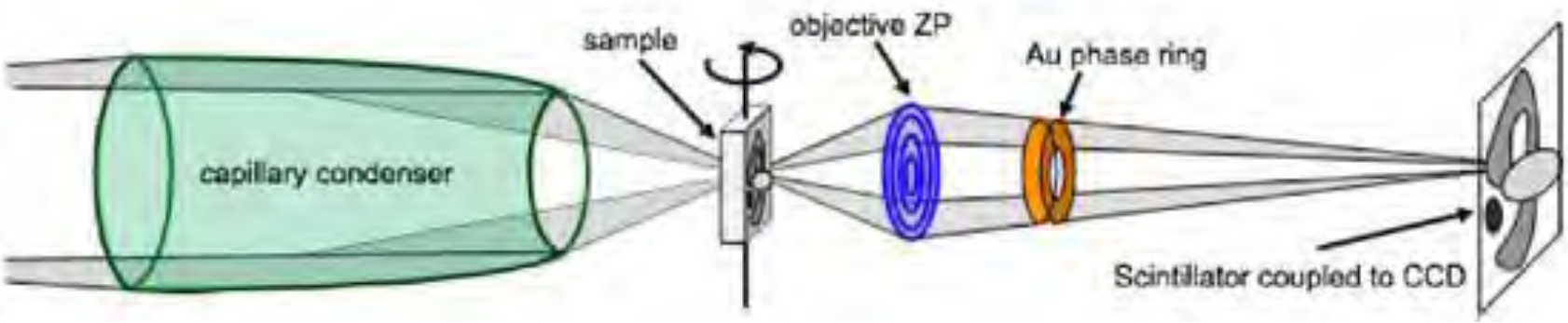

Beam collected onto sample

Viewed by zp

Image is magnified

Rotate sample→ tomography
Absorption contrast
Phase contrast

Technical Specifications

1) X-ray energy range

Capable operation between energy range 5-11keV for absorption contrast mode (optimized at 8keV);

Two discrete energies 5keV and 8keV for Zernike phase contrast mode.

2) Resolution

Sub-30nm in high resolution mode with 20um * 20um field of view;

Sub-50nm resolution for 40um * 40um field of view.

3) Imaging modalities

Absorption contrast;

Phase contrast

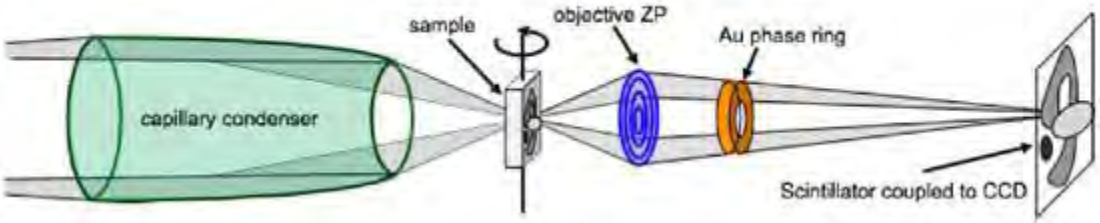

4) Data acquisition and reconstruction

Automatically acquire tomographic projection datasets;

Align the projection;

Reconstruct the 3D dataset.

Transmission X-ray Microscope at X8C, NSLS

- **Markerless automatic nano-tomography**
- **Local tomography**
- **XANES imaging**

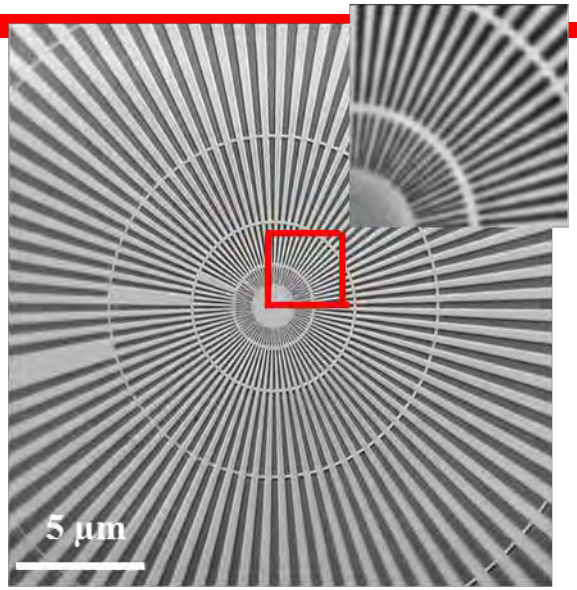

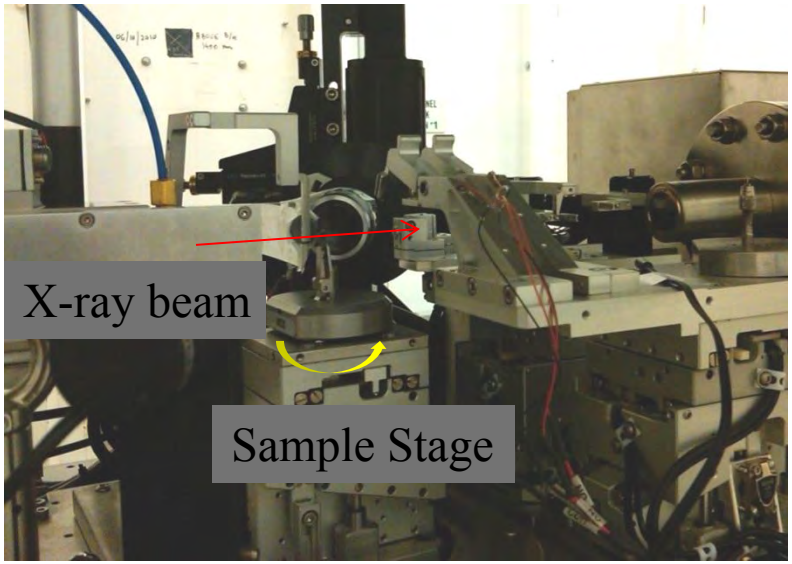

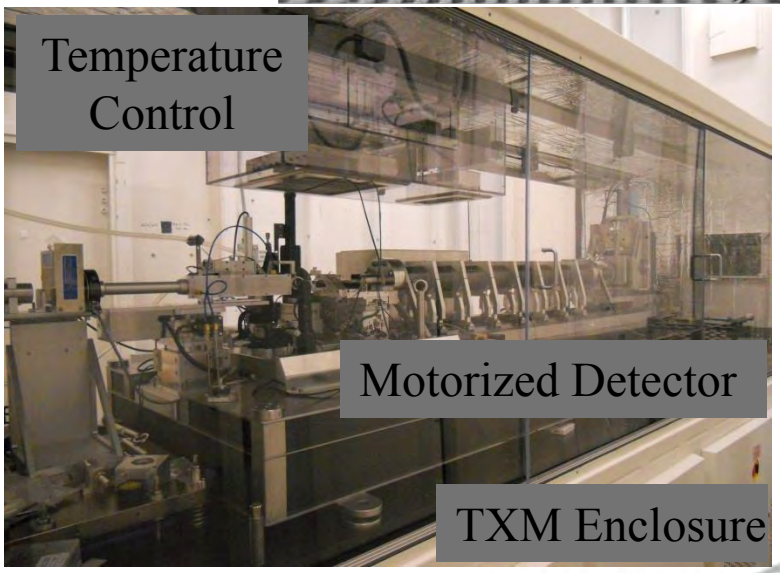

J. Wang et. al. *Appl. Phys. Lett.* 100, 143107 (2012)

Unique Capabilities

Automated Tomography

Correct wobble generated during rotation

- Ball-bearing rotation stage → reduce the rotation wobble
- Passive rotational run-out correction system: a precision cylinder mounted on a low run-out ball bearing rotation stage, 3 integrated capacitive sensors→ measure the residual run-out → calibrated through sets of tomography data from a standard→ converted to $\Delta x\ (\theta)$ and $\Delta y\ (\theta)$ →automatically applied to each 2D projection

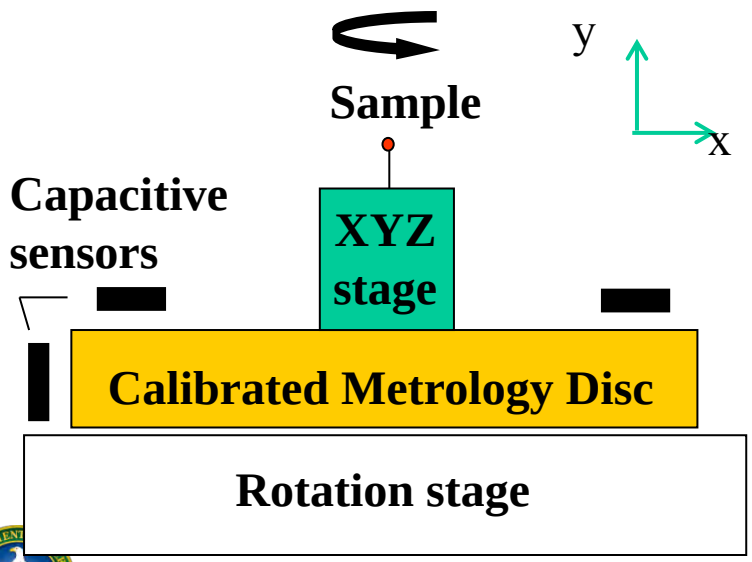

Over 1000 images for reconstruction

Jun Wang, et.al. "*Automated Markerless Full Field Hard X-ray Microscopic Tomography at Sub-50 nm 3D Spatial Resolution*" ---***Appl. Phys. Lett. (100, 143107, 2012)***

Unique Capabilities

Local Tomography

Motorized and encoded sample translation stage above the sample rotation stage → easily move any part of the sample to rotation axis
Combined with autotomography→ local tomography

Interesting region → 2D mosaic images at 0 and 90 degrees→ center of rotation axis.

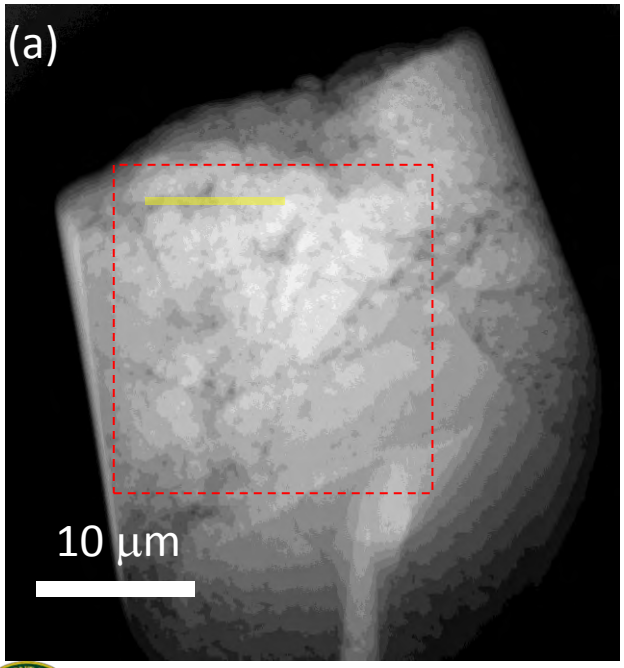

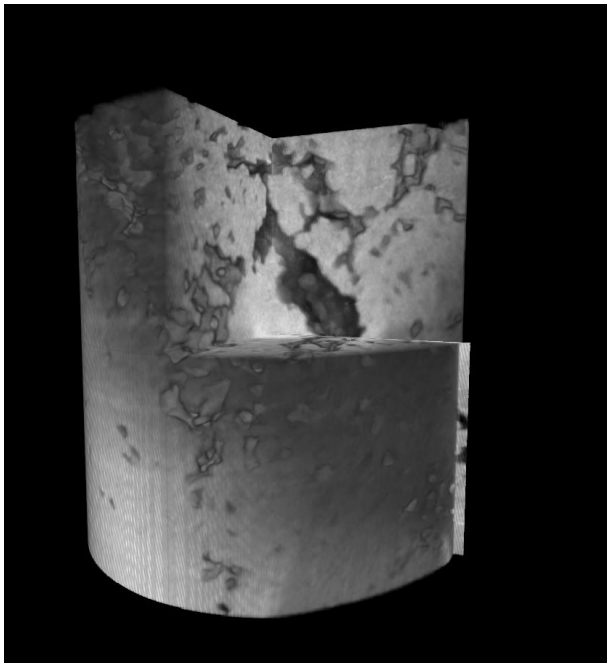

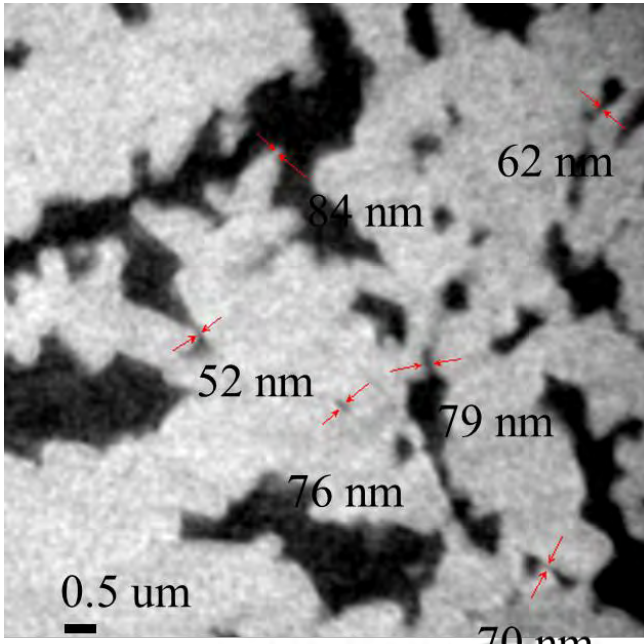

Unique Capabilities

Spectroscopic Imaging

Motorized detector translation stage→ detector distance adjustable→ constant magnification→ best resolution spectroscopic imaging

LiCoO2(LCO) and Li(Ni1/3Mn1/3Co1/3)O2(NMC)

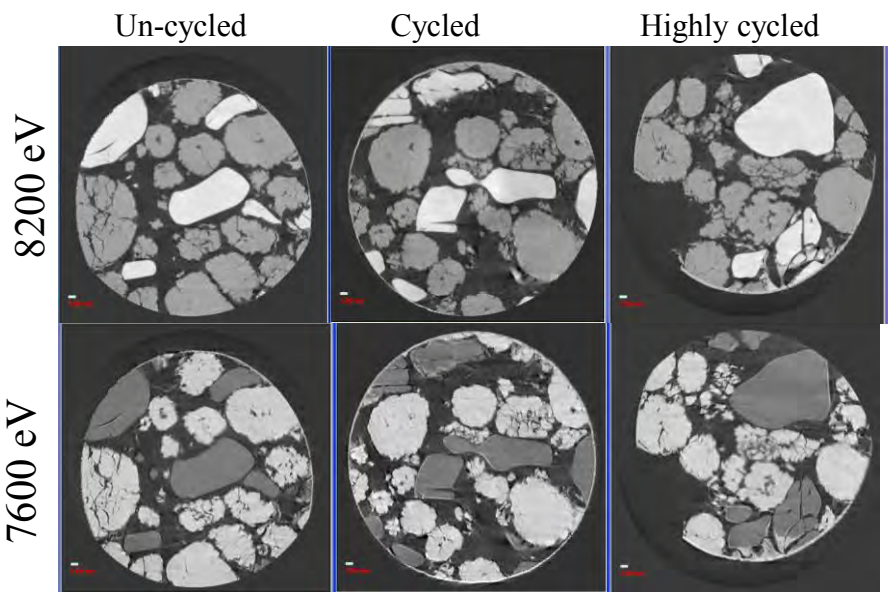

Yu-chen Karen Chen-Wiegart,et.al, ***Elecctro. Comm. (28, 2013)***
Zhao Liu, et al, ***J. Power Source (227, 2013***)

Nickel-yttriastabilized zirconia (Ni-YSZ)

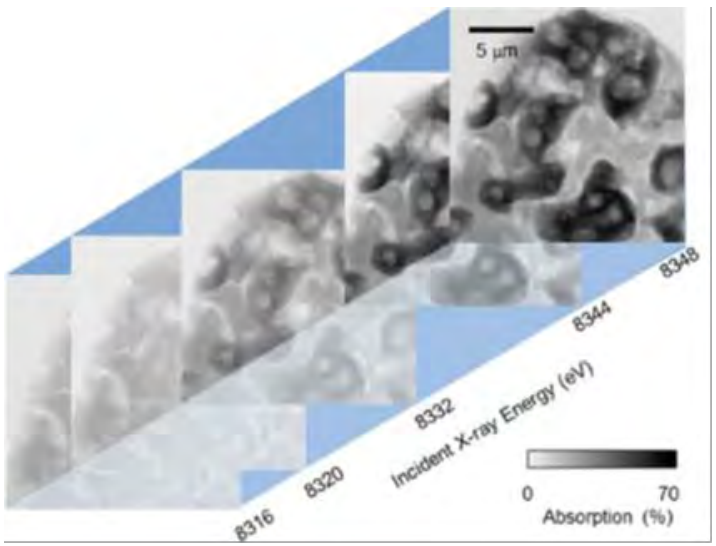

Yu-chen Karen Chen-Wiegart,et.al, ***Appl. Phys. Lett. (101, 253901, 2012)***

In-Situ Chemical Mapping of Lithium-ion Battery Using Full-field Hard X-ray Spectroscopic Imaging

- First time in-situ study on battery materials with non-destructive and quantitative characterization of the phase and chemical state as well as morphology evolution at nanometer resolution during cycling using spectroscopic imaging TXM-XANES.
- First demonstrated a core-shell conversion model
- First revealed an interface phase following the lithiation-delithiation process
- First directly observed a size-dependent lithiatoin-delithation process

CuO represents a typical conversion mechanism evolution

$$M_xO_y + 2y\,Li^+ + 2ye^- = yLi_2O + xM$$

- Modified coin cell with two Kapton windows
- Replacing conventional metal foil with carbon paper as the electrode support

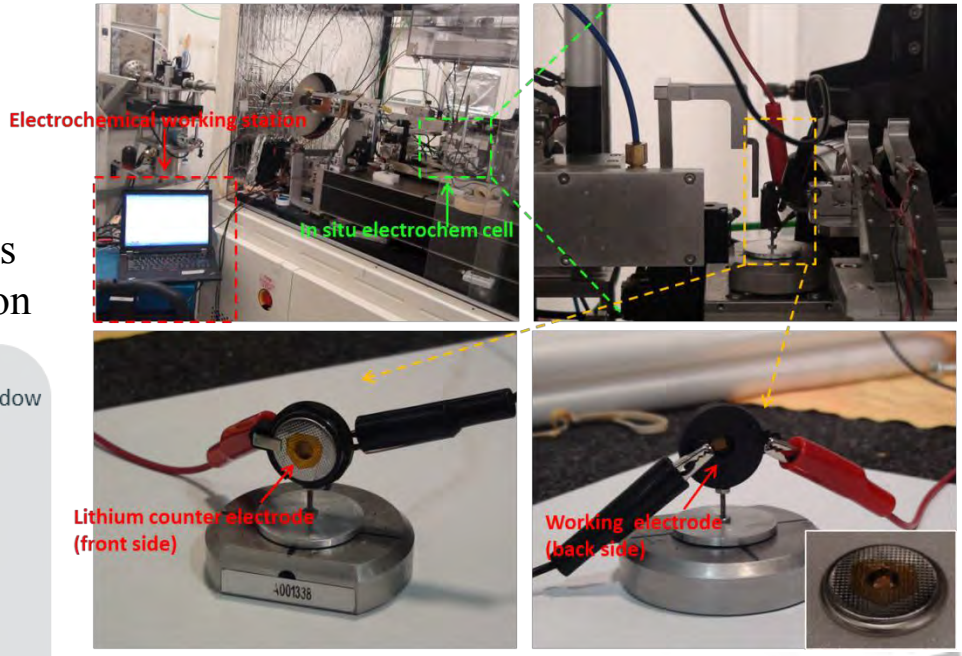

U.S. DEPARTMENT OF ENERGY

BROOKHAVEN NATIONAL LABORATORY
BROOKHAVEN SCIENCE ASSOCIATES

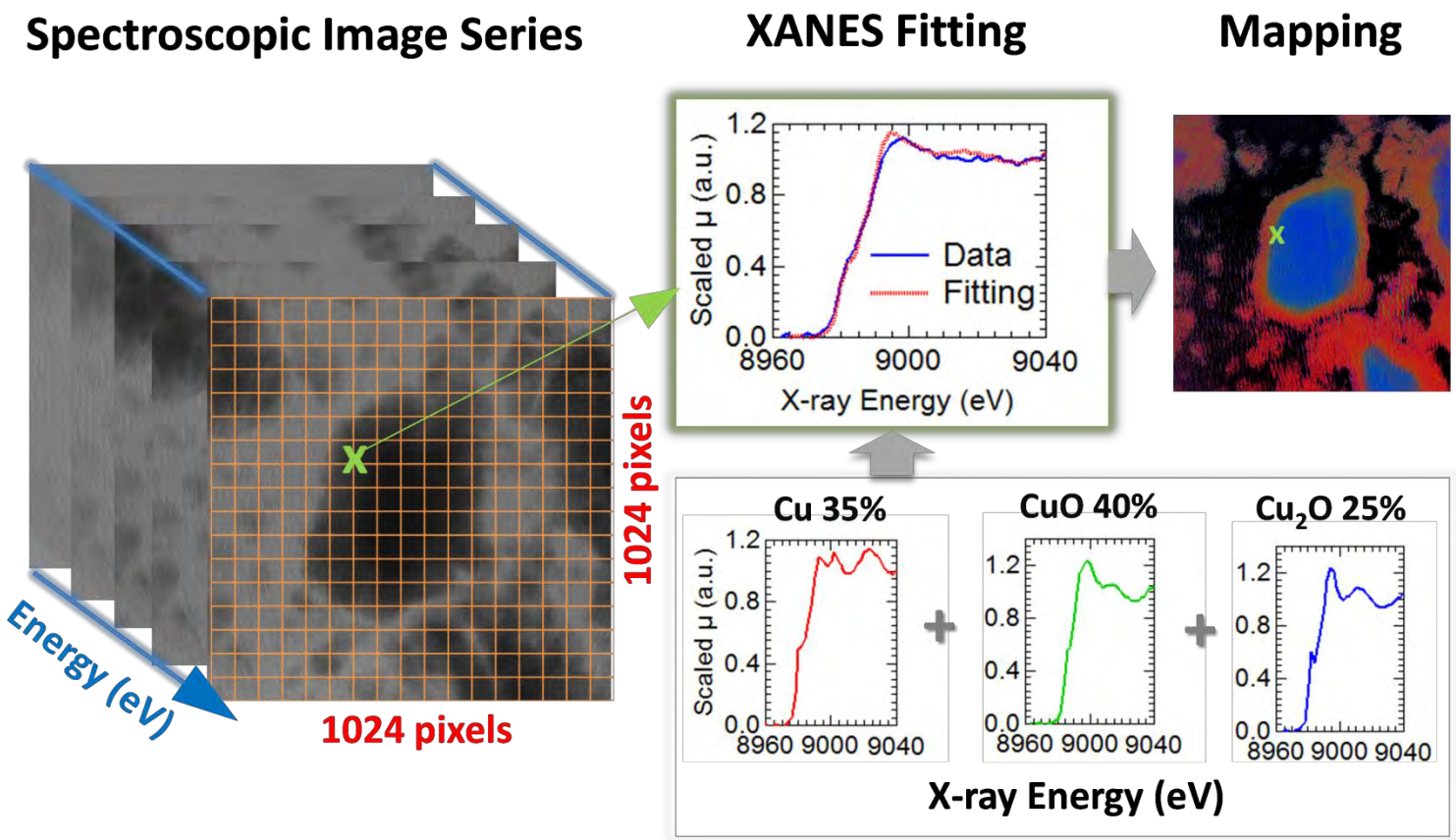

Principles and data processing for TXM-XANES measurements

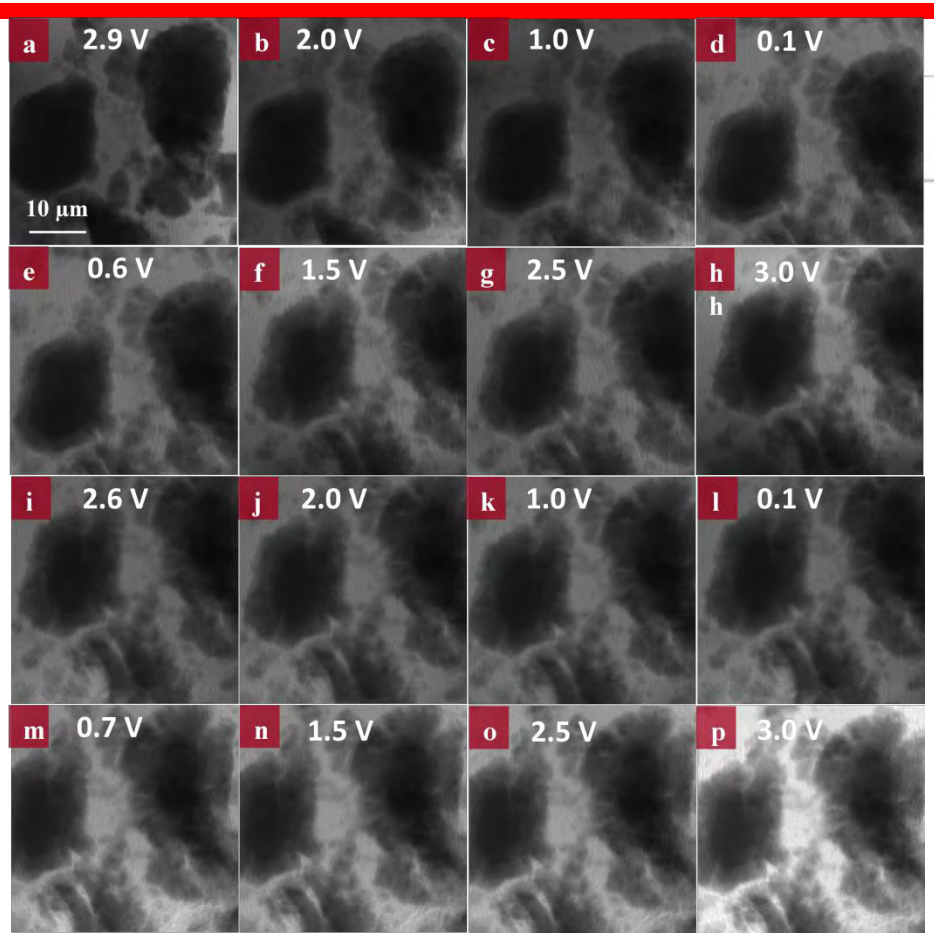

The morphology evolution of CuO electrode during the first (a-h) and second cycle (i-p)

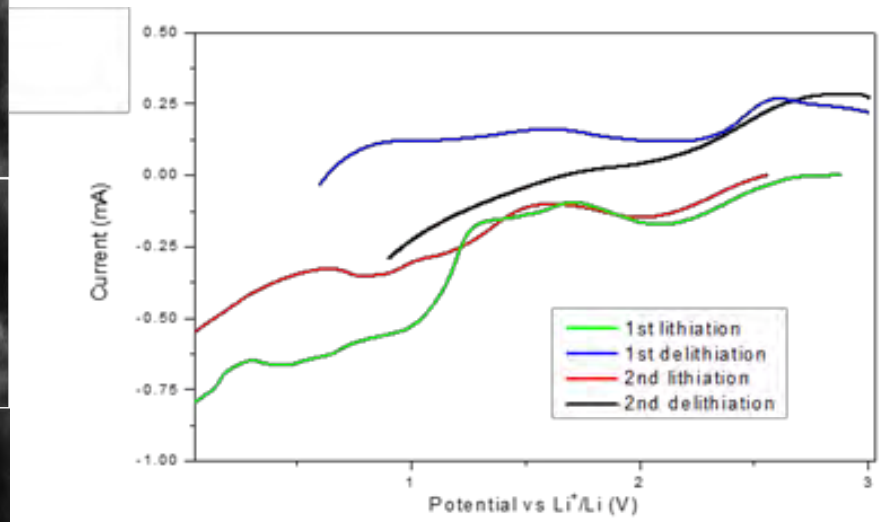

Corresponding electrochemical measurement:

Cyclic voltammetry curves during the first two cycles at different potentials for CuO electrode

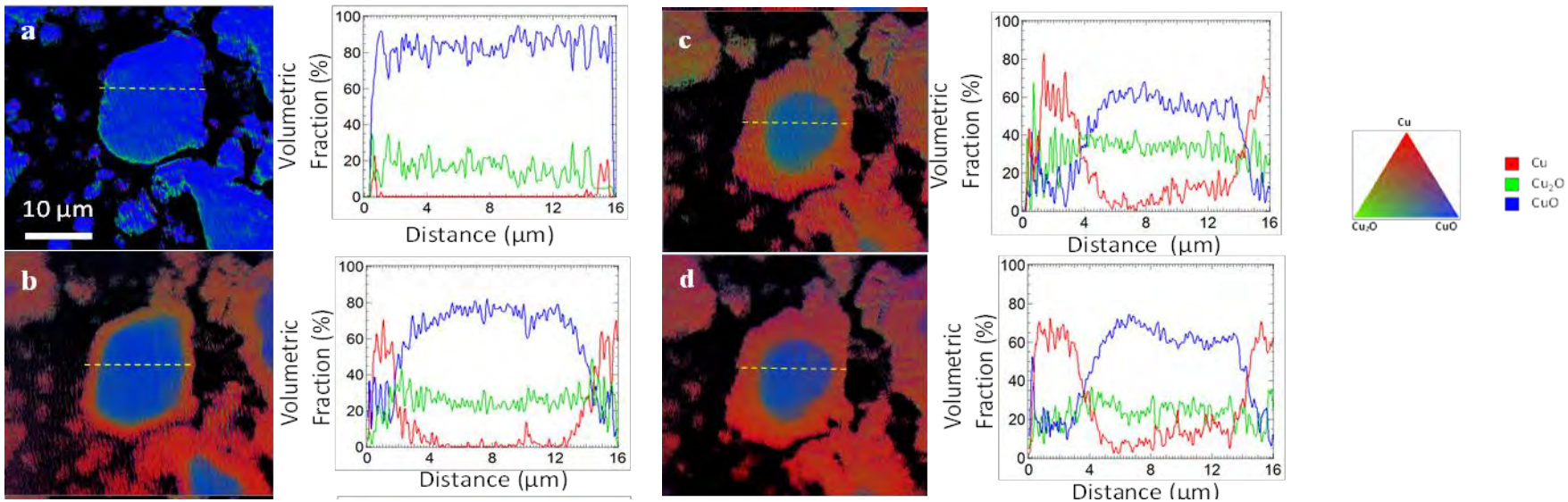

Chemical phase mappings of CuO during cycling, and Line profile of the corresponding particle during cycling.

(a) fresh sample: a major CuO with a small amount of Cu_2O

(b) 1st lithiated sample: a core (CuO)-shell (Cu) structure with an interface phase (Cu_2O)

(c)Rest and 1st delithiated sample: self-reaction during the rest period (the rising of open circuit potential), and the following delithiation to form Cu_2O (anodic scanning)

(d) 2nd lithiated sample: some Cu_2O in the shell (green) was reduced to Cu (red), and the line profile shows a decrease of Cu_2O

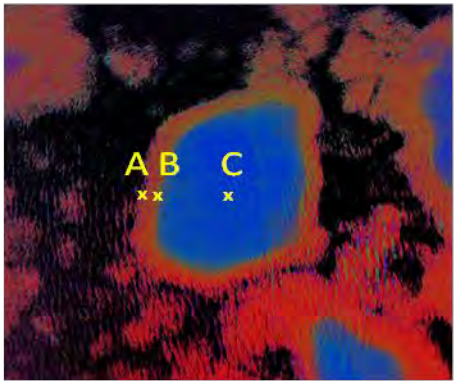

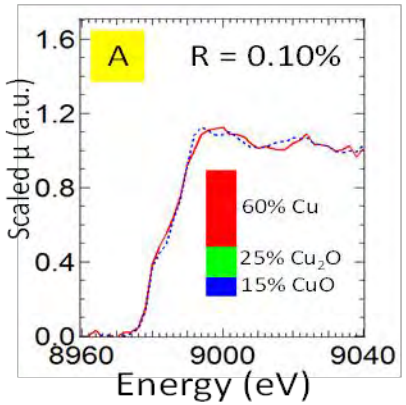

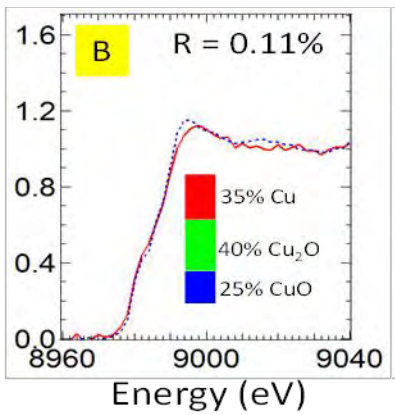

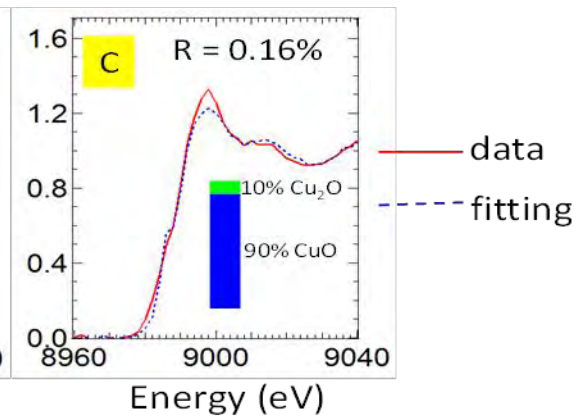

Phase composition upon the first lithiation at the selected zones

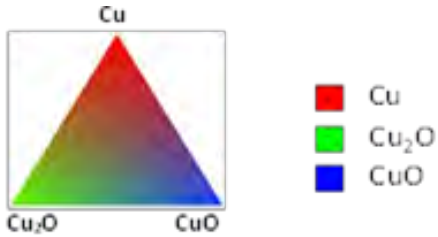

the XANES spectra and the best fitting results at three representative locations—shells, interface, and core—of the first lithiated sample

Surface: 60%Cu, 25%Cu2O, 15%CuO

Interface:35%Cu, 40%Cu2O, 25%CuO

Core: CuO (90% CuO, 10% Cu2O)

- in situ TXM imaging and XANES phase analysis were used to elucidate in situ the conversion reaction mechanism of a typical lithium-ion battery material, CuO.
- The morphology evolution, chemical phase change, and detailed composition information on CuO anodes strongly suggest a size-dependent and core–shell lithiation–delithiation mechanism.
- The morphology evolution during the rest period suggest that the volume change in anode materials may also originate from Li ion diffusion and equilibrium, particularly for large particles.
- The information presented in this work will be a key for further modelling, simulation and design of new electrode materials

In situ chemical mapping of a lithium-ion battery using full-field hard X-ray spectroscopic imaging†

Jiajun Wang, Yu-chen Karen Chen-Wiegart and Jun Wang*

Chemical Communications 49 *(2013) 6459–6566*

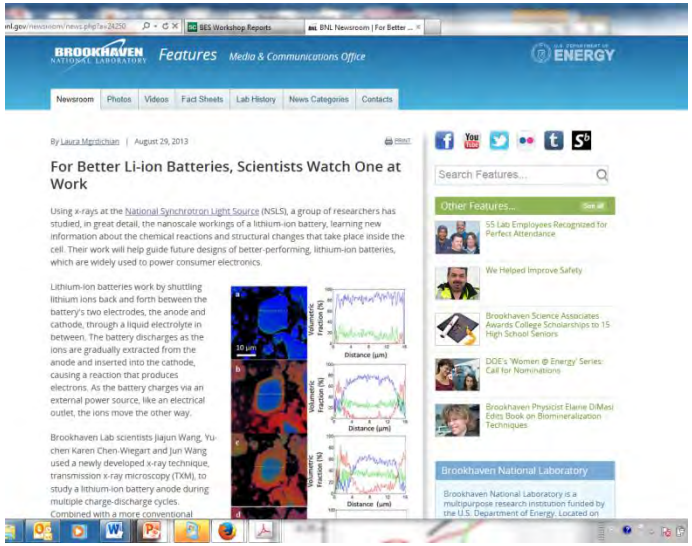

Featured as inside cover

Science highlight on BNL website

Oral presentation at ECS meeting 2013

U.S. DEPARTMENT OF ENERGY

BROOKHAVEN NATIONAL LABORATORY
BROOKHAVEN SCIENCE ASSOCIATES

In Situ Synchrotron X-Ray Nanotomography of the (De)lithiation Processes in Tin Anodes

Lithium-ion batteries (LIBs) are based on insertion reaction chemistry which introduces microstructural changes into host materials by lithiation and delithation process. The changes are particularly pronounced in some high-capacity anode materials such as silicon- and tin-based anodes, leading to large volume change, fracture, and pulverization thereby reducing the battery capacity and cycle life. However, the mechanism of the degradation has not been fully understood yet.

For the first time a non-destructive in situ x-ray nano-tomography:

- Monitor the 3D microstructural changes in the electrode at the nanoscale,
- Quantitatively analyze the 3D microstructural changes (including volume change, feature size, specific area, and curvature) from the high-quality data
- Correlate the morphological changes with the electrochemical reactions and to evaluate the stress on the electrode particles that is induced by the lithiation and delithiation processes

A key component is a micro- electrochemical cell

- 180 degree rotation without blocking beam
- Micron scale on the studying material within beam
- Closed system with electrode immersed completely in electrolyte to allow reactions in three dimensions
- function normally as a working battery
- electrochemical measurement (CV and charge/discharge profile)

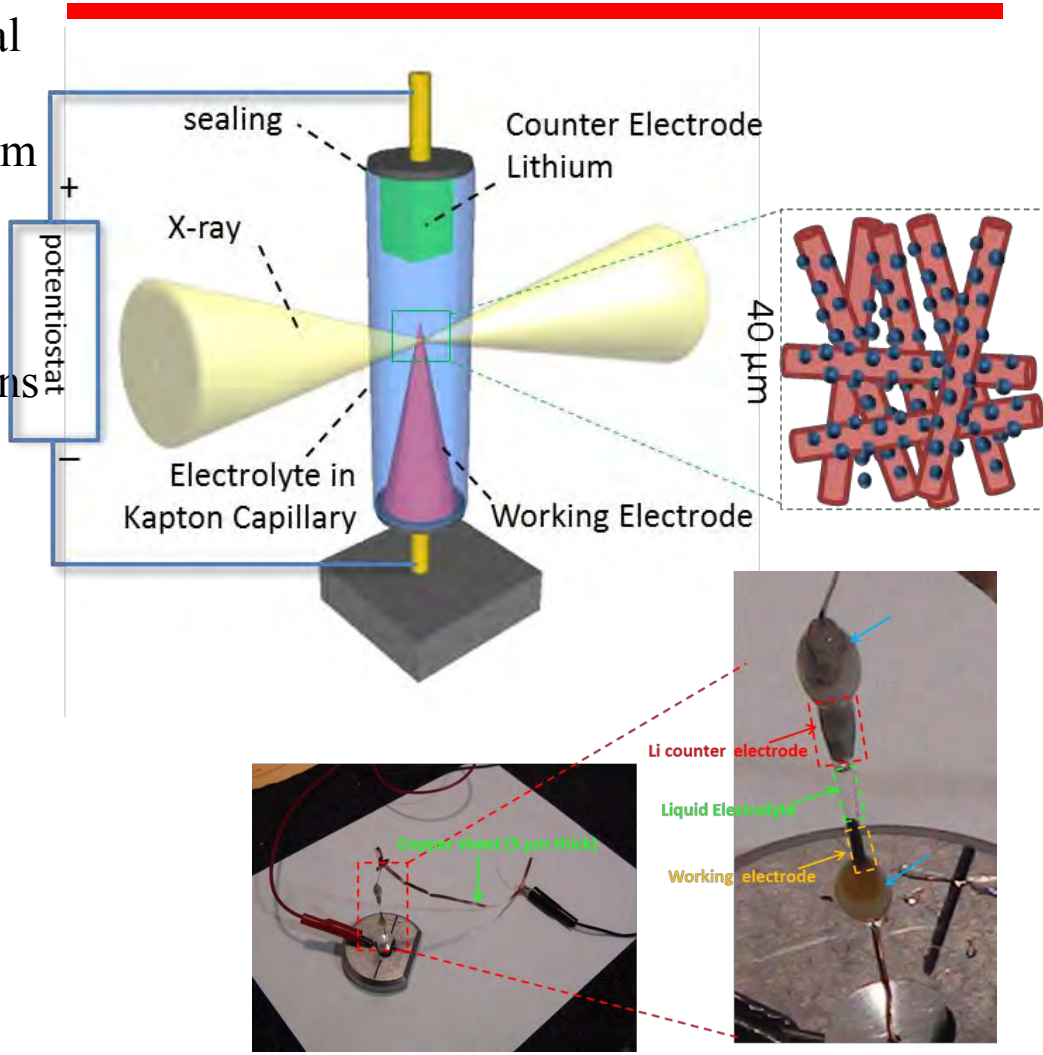

Challenging:

- Limited working distance
- coin cell insufficient
- transparent supporting material along the beam path
- proper sealing for repeated cycling

The complexity of developing the cell has hindered the investigation of in situ 3D microstructural evolution using TXM.

Sn particles as an anode, a commercial carbonate electrolyte, and lithium metal as a counter/reference electrode.

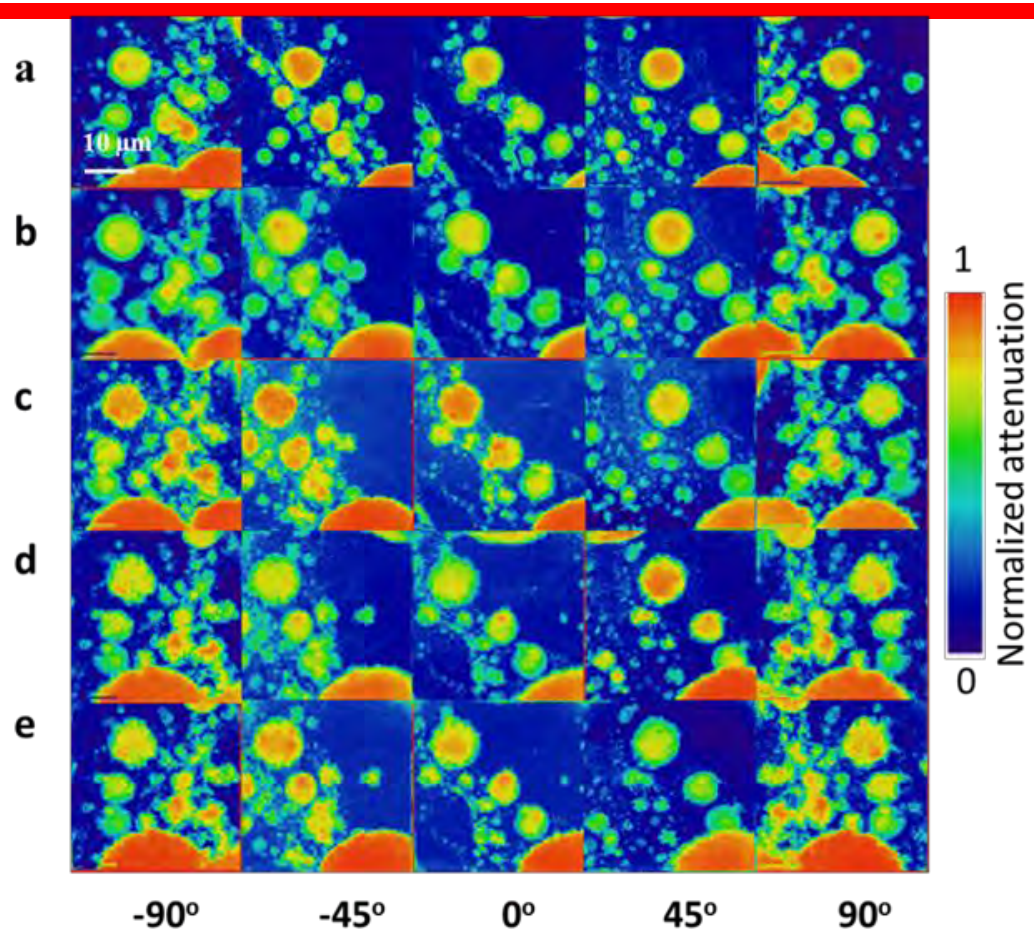

Selected 2D TXM projections from -90 to 90 at each stage of the lithiation-delithition process.
a, fresh sample
b, after1st-lithiation
c, after 1st-delithiation
d, after 2nd lithiation
e, after 2nd delithiation.
Note the significant changes expansion, shrinkage, cracks and pulverization during the 1st delithiation and 2nd lithiation on the representative particles.

particularly remarkable at some curved and coarse surface of particles due to high stress formation and release, as some voids were created there. some surface mechanical degradation is not visible from other angles of view, indicating the volume change of Sn particles is anisotropic.

The electrochemical performance of Sn anode materials

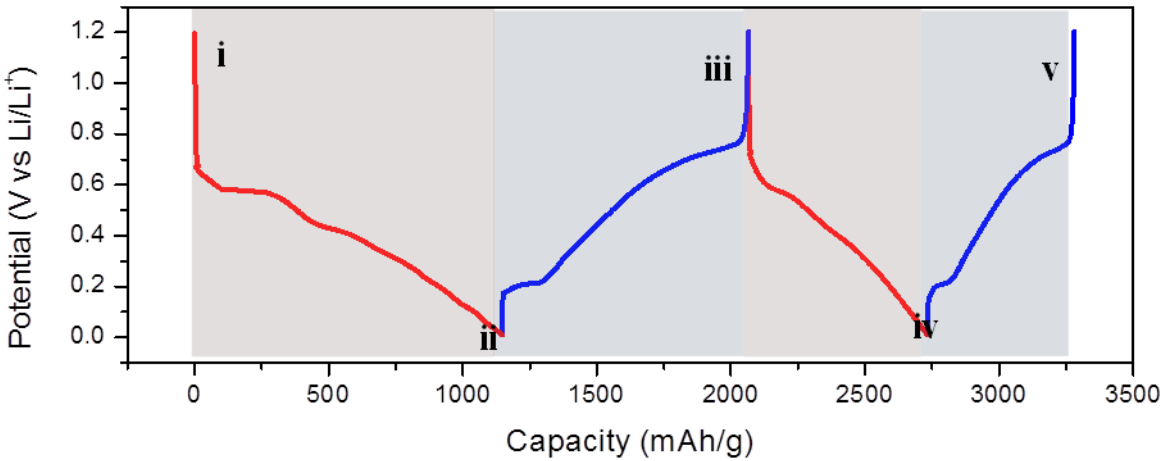

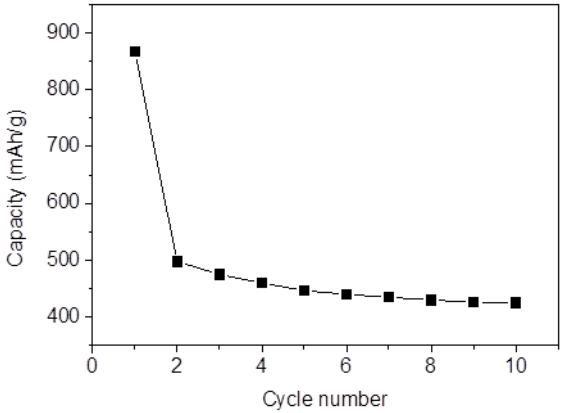

the charge/discharge profile of Sn anode at a current density of 10 mA/g in a voltage range of 0.005-1.2V at the first two cycles

the reversible discharge performance of the initial ten cycles.

After deducting the capacities from electrolyte's decomposition and carbon paper's contribution, the first discharge capacity is 867.2 mAh/g, which is close to the theoretical capacity of Li4.4Sn (993 mAh/g). The second discharge capacity is decreased to 489 mAh/g due to the mechanical degradation. After these initial two cycles, the Sn anode shows a stable discharge capacity and reversibility

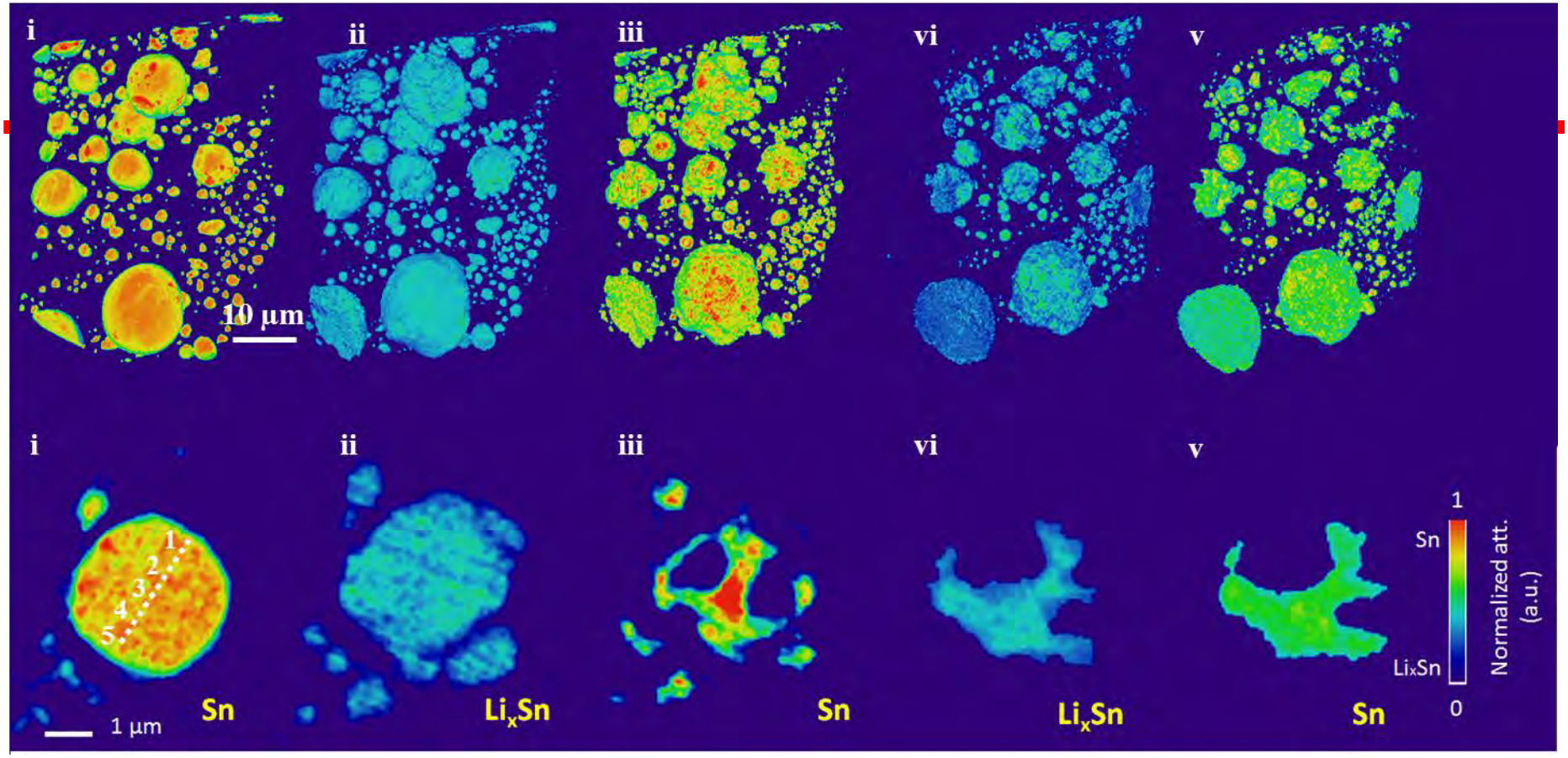

(a) 3D morphological evolution of Sn particles and (b) Pseudo Cross-section chemical images of a single Sn particle at the first two lithiation-delithiation cycles.

1st lithation:Volume expansion and initial cracking, but overall structure intact
1st delithiation: Severe pulverization and facture, when Li ion exacting and volume shrinking
2nd lithation: several pulverization and fracture continue
2nd delithation: No significant changes develop, reach structural equilibrium
The particle shows severe fracture and pulverization at the initial stage of cycling, but stays mechanically stable after that while electrochemical reaction still goes on reversibly

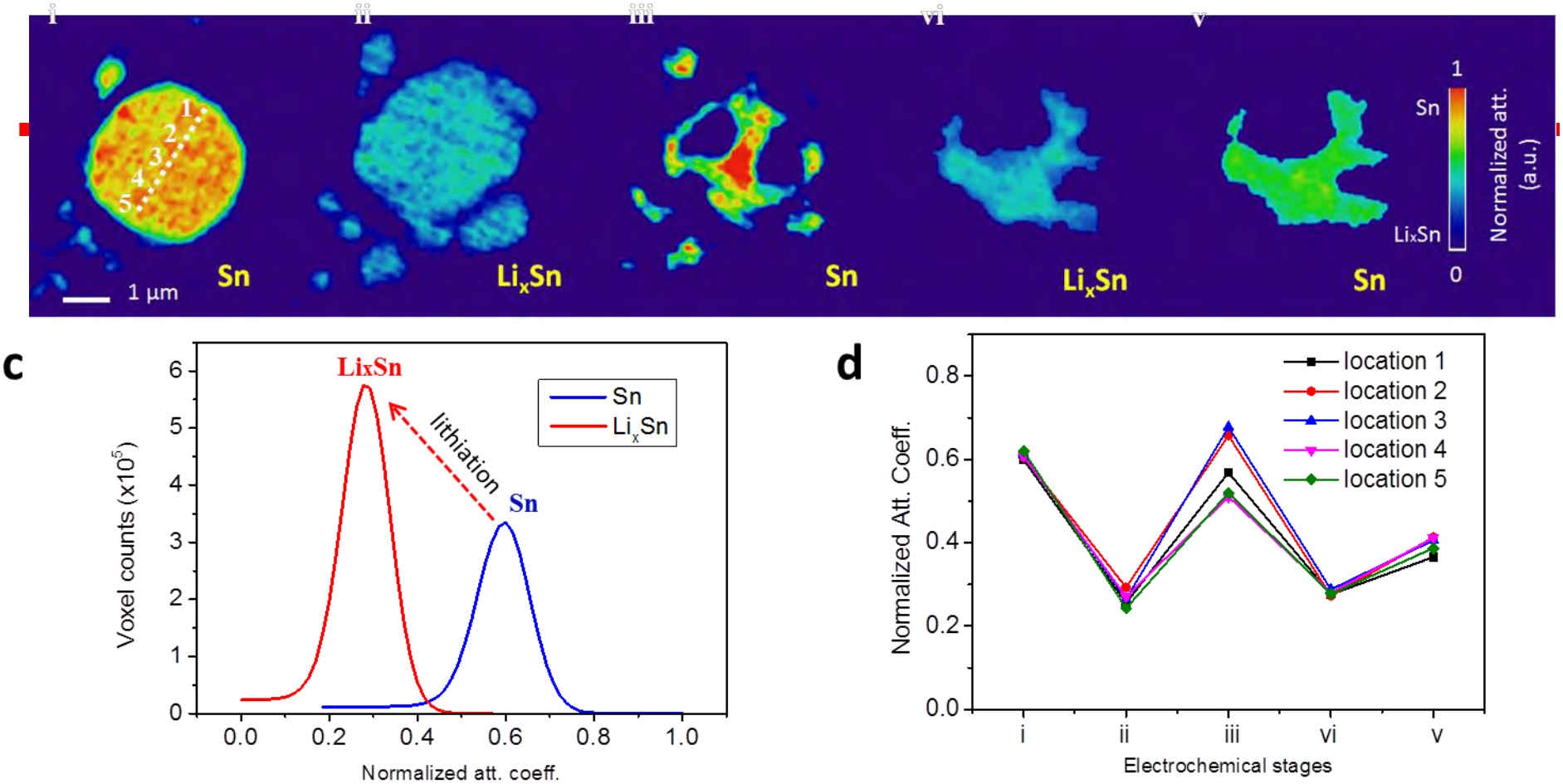

The color scale corresponds to the normalized linear att. coeff of the materials, direct visualization of chemical information

1st lithiation: Normalized att. coeff. decrease from Sn to LixSn, nearly full lithiation reaction
1st delithation: inhomogeneous mass distrubution, high att coeff in core
2nd lithiation/delithation: continuing att coeff change confirms reversible reaction

well consistent with the electrochemical cycling measurements. The correlation of morphology and chemical information clearly indicates that Sn anodes reach a structural equilibrium after the mechanical degradation stages at the initial electrochemical cycling.

Quantitative 3D morphological analysis of the electrode undergone electrochemical cycling

	fresh	after 1st lithiation	after 1st delithiation	after 2nd lithiation	after 2nd delithiation
volume of Sn particles (nm^3)	4.85E+11	7.72E+11	5.87E+11	7.05E+11	6.88E+11
absolute volume change of Sn (%) (compared to fresh)	100	159	121	145	142
relative volume change(%) (after each half-cycle)	--	+59	-24	+20	-2
surface area (nm^2)	0.98E+09	1.62E+09	1.63E+09	2.61E+09	2.59E+09
specific area (nm^{-1}) S_y	0.00201	0.00210	0.00277	0.00370	0.00376
specific area change(%) (compared to fresh)	100	104	138	184	187
relative specific area change (%) (after each half-cycle)	--	+4	+32	+33	+2
1/specific area (nm), S^{v-1}*	496.9	476.2	360.7	270.3	265.9
absolute feature size change (%) (compared to fresh)	100	96	73	54	54
relative feature size change(%) (after each half-cycle)	--	-4	-24	-25	-2

Specific area: defined as the surface area per unit volume

1/specific area: a parameter to characterize averaged feature size

3D Quantitative Analysis

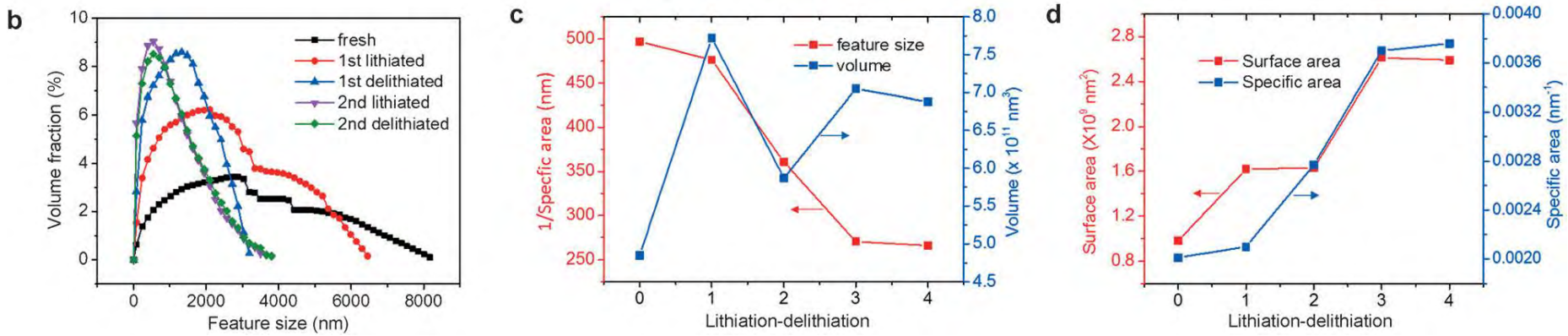

- Low volume expansion attributed to a carbon coating acts as a buffering layer on Sn
- Surface area subject to combined effect of volume change and pulverization, two opposite factors keep the surface area constant during the delithiation
- Specific area, a parameter to quantify the fracture. Rapid increase during the first delithiation and the second lithation further reveals the dominant roles of these two stages in the fracture of the material

Curvature distributions at different lithiation-delithiation stages

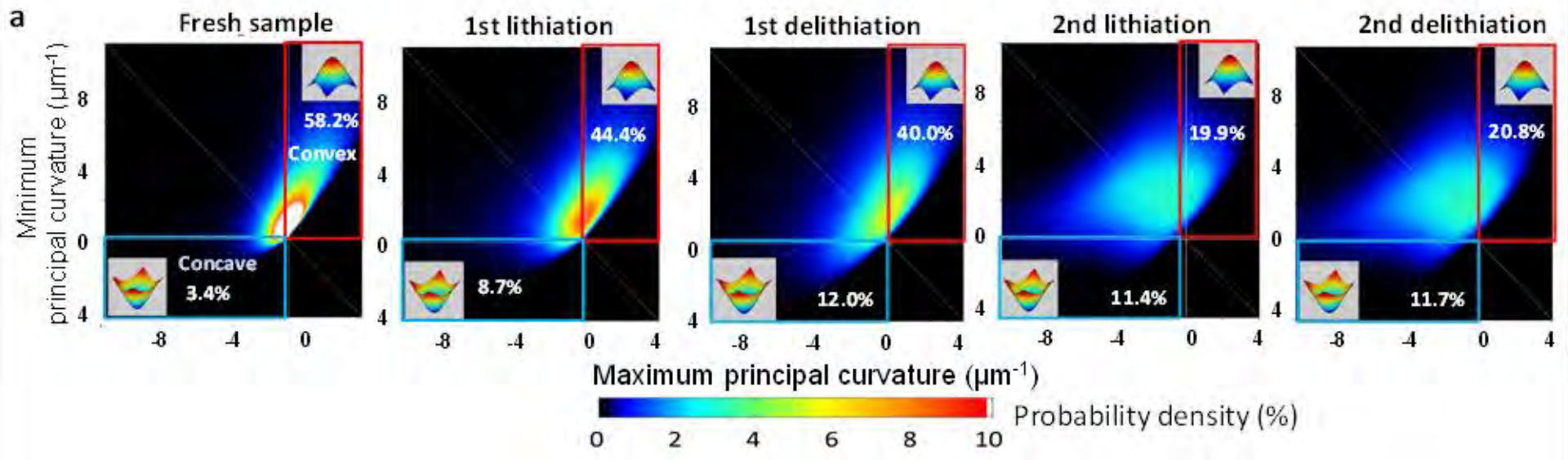

- Geometric characteristics effect on stress induced by the lithation-delithation process
- Curvature distribution, interfacial shape distribution (ISD), calculated on all particles
- Concave features increased significantly after the first lithiation, lead to fracture and pulverization during the first delithiation
- Further induced structural instability in the second lithiation
- Shape of the particles changed significantly after 2nd lithiation
- Convex features dropped 50%, which helped the particles to reach a dynamic structural stability.

Surface morphology evolution and internal microstructural changes of an individual particle.

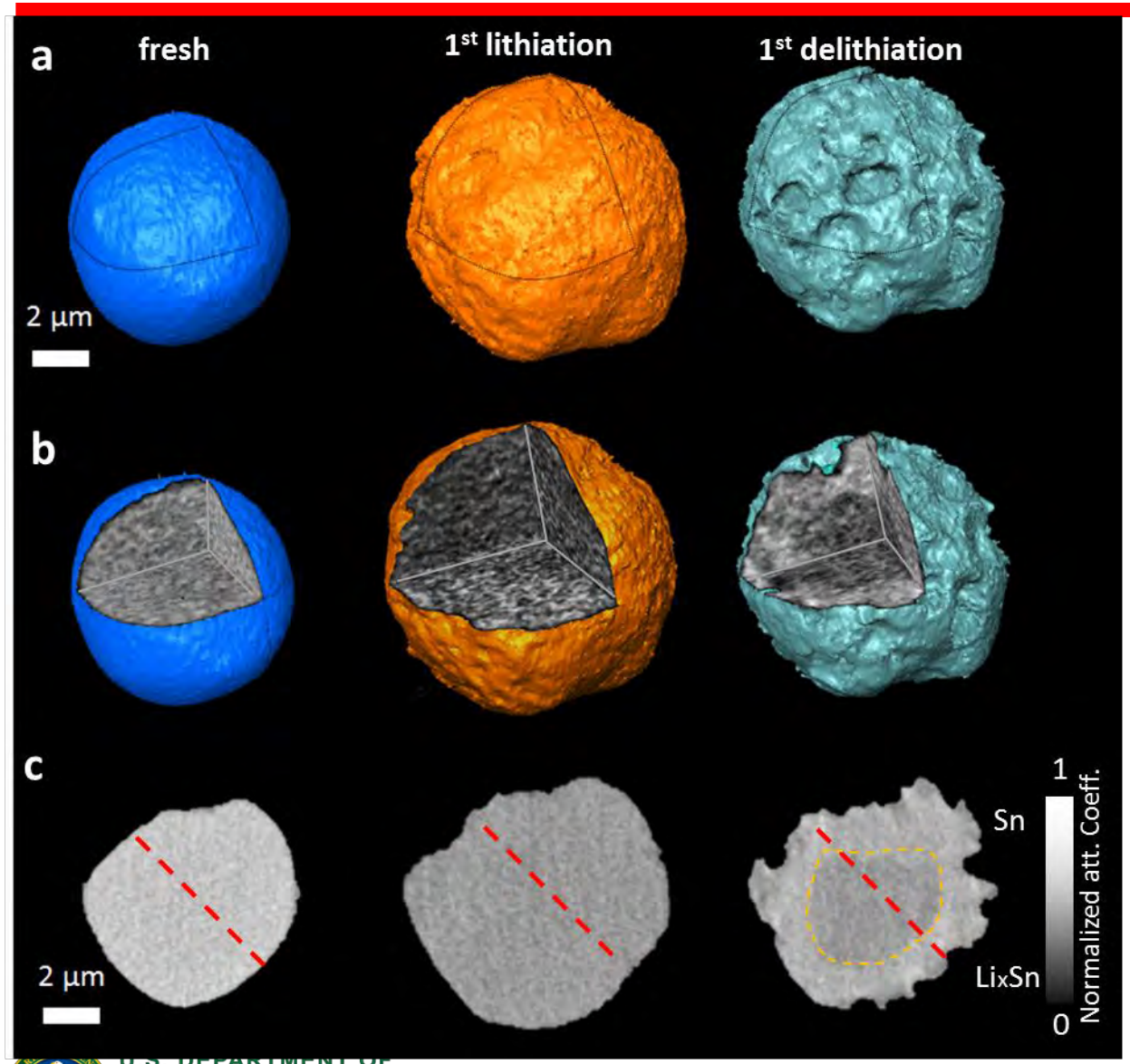

a) Surface morphology evolution of the particle

b) Internal microstructure of the same particle with a cut view

c) Cross-sectional image showing the chemical phase distribution

- a clear volume expansion during the lithiation and a severe morphology pulverization during the delithiation process
- a pronounced attenuation contrast between core and shell, indicating a partial delithiation in this large particle

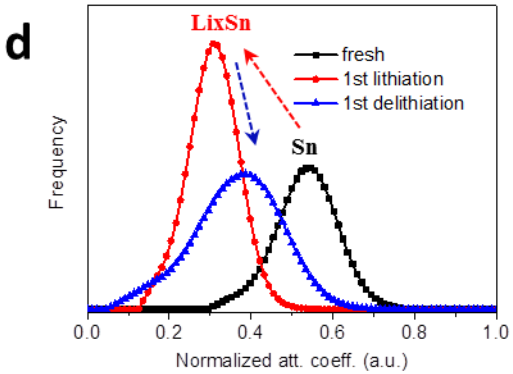

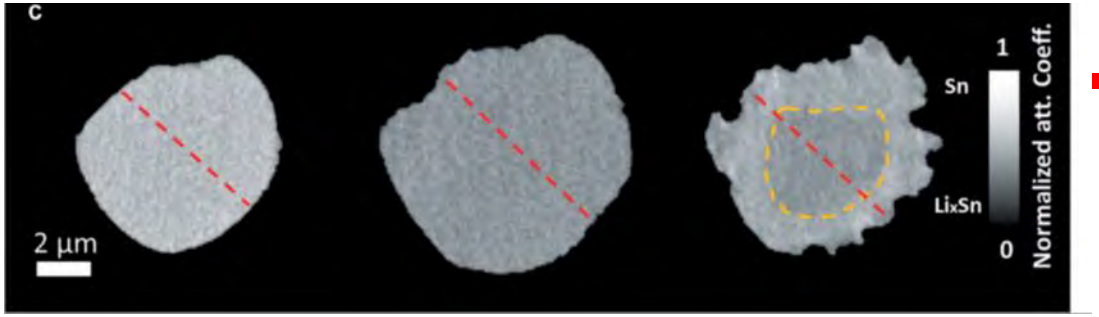

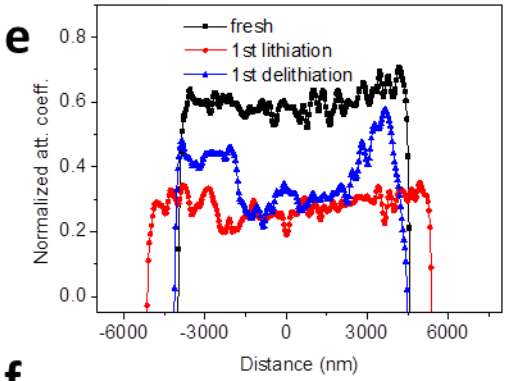

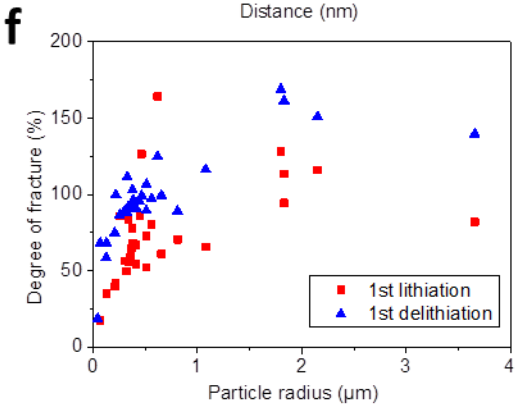

d) Normalized attenuation coefficient histogram of the cross section during the first cycle

Lithiation: volume expansion →large area; peak shift→ chemical composition change

e) Line scanning profile of the normalized attenuation coefficient for the cross section

Exhibit the same trend

f) Statistical information of size-dependent effect on fracture within Sn particles

degree of fracture: the increase in the specific area in comparison with a particle without fracture undergone the same volume change

- Provide a direct way to look inside the electrochemical reaction of batteries to better understand the mechanism of structural degradation
- Suggest that better control of the initial electrochemical cycle to minimize fracture and pulverization is critical for retaining electrode performance in the following cycles
- Guide the engineering and processing of advanced electrode materials
- Produce accurate 3D parameters for theoretical simulations and modeling
- The developed micro-electrochemical cell and the methodology can be widely applied in a variety of energy storage, material science and chemistry field, well beyond the specific battery example in this work.

Angewandte

Chemie

Angew. Chem. Int. Ed. 2014, 53, 1 – 6 2014 Wiley-VCH Verlag GmbH & Co. KGaA, Weinheim

In Situ Three-Dimensional Synchrotron X-Ray Nanotomography of the (De)lithiation Processes in Tin Anodes**

Jiajun Wang, Yu-chen Karen Chen-Wiegart, and Jun Wang*

Press Release, BNL news, Office of Science for DOE news

This work was supported by a Laboratory Directed Research and Development (LDRD) project at Brookhaven National Laboratory.
Use of the NSLS was supported by the U.S. Department of Energy, Office of Basic Energy Science (DE-AC02-98CH10886).

U.S. DEPARTMENT OF ENERGY

BROOKHAVEN NATIONAL LABORATORY
BROOKHAVEN SCIENCE ASSOCIATES

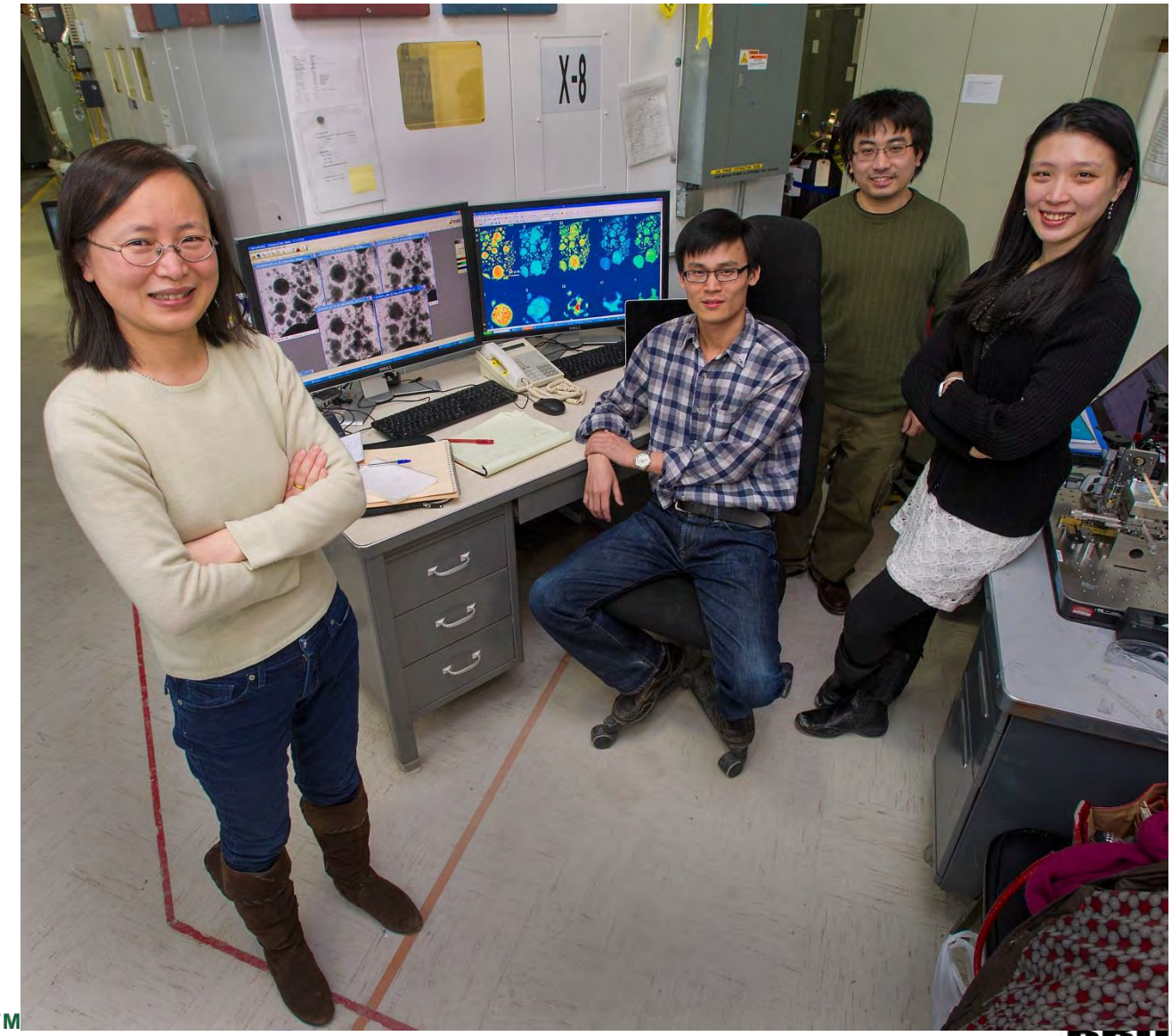
X-8